Nyman, Leo; Kukko, Kirsi; Kestilä, Antti; Myllymäki, Vesa; Lohilahti, Jarkko; Kumpulainen, Joni; Vehkamäki, Marko; Salmi, Mika; Lafont, Ugo; Kallio, Esa

Overview of ground-based testing of components made from electrically-conducting doped peek for space applications

Published in:
Proceedings of the 20th European Conference on Composite Materials - Composites Meet Sustainability

Published: 12/12/2022

Document Version
Publisher's PDF, also known as Version of record

OVERVIEW OF GROUND-BASED TESTING OF COMPONENTS MADE FROM ELECTRICALLY-CONDUCTING DOPED PEEK FOR SPACE APPLICATIONS

Leo Nyman[a], Kirsi Kukko[a], Antti Kestilä[b], Vesa Myllymäki[c], Jarkko Lohilahti[d], Joni Kumpulainen[d], Marko Vehkamäki[e], Mika Salmi[a], Ugo Lafont[f], Esa Kallio[a]

a: Aalto University, FI-00076 Aalto, Finland. Email: leo.nyman@aalto.fi
b: Finnish Meteorological Institute, Finland.
c: Carbodeon Ltd, Finland.
d: Maker3D Ltd, Finland.
e: University of Helsinki, Finland.
f: European Space Research and Technology Centre, Netherlands.

Abstract: *Additive manufacturing (AM) has shown to be a promising method for creating high-performance plastic components. In space, harsh environmental conditions such as vacuum ultraviolet radiation and significant temperature changes cause the degradation of polymers and static electricity buildup on the surface of non-conductive components.*

This study explores geostationary orbit communication-satellite parts additively manufactured using doped polyether ether ketone (PEEK). Several spacecraft parts were selected for detailed redesign and additive manufacturing. These parts are commonly used in communication satellites and belong to secondary structures that need not withstand heavy forces.

The effects of the space environment on the doped PEEK material and its properties were studied in ground-based laboratories. The printed parts were mechanically and functionally tested. Low-mass space-grade components can be made with this method and material combination while conforming with the stiffness requirements for secondary spacecraft structures. This manufacturing method aims to achieve mass savings of 50% compared to metallic baselines.

The analysis showed that that printing parameters used in the fused filament fabrication (FFF) process significantly affect the mechanical performance of the parts. Moreover, the high strength and stiffness of the FFF-printed carbon-fibre doped PEEK brackets was found to make them ideal for joints used in spacecraft honeycomb panel structures, enabling up to 25–50% savings in bracket mass. Overall, the used FFF manufacturing method enables fast, and cost-effective low batch-size production runs.

Keywords: PEEK; Additive manufacturing; thermoplastic composites; spacecraft; material extrusion

1. Introduction

Spacecraft secondary structures must withstand loads that are atypical for terrestrial use cases. One of the most important aspects to consider here is the stiffness of the assemblies that make up the secondary (and primary) structures in a spacecraft. This requirement arises from the vibration-induced acceleration loads during a launch. Most rockets have a vibration-spectrum that favors having as-stiff-as-possible structures to eliminate low resonant frequencies, leading

  doi:10.5075/epfl-298799_978-2-9701614-0-0

to high mechanical loads. By designing high-stiffness structures, their mass can be kept as low as possible – an important aspect when considering the high cost of mass to orbit.

The design of high-stiffness structures from plastics is challenging, but the solution possibly resides in the use of dopants, topology optimization [1] and additive manufacturing [2]. The dopants could also help in solving other major challenges facing the use of plastics in space, such as surface charging and their susceptibility to vacuum ultraviolet (UV) light, radiation, and atomic oxygen. The surface charging issue can be decreased by increasing the electrical conductance of the material. Currently, UV-resistant plastics are common in terrestrial applications and are manufactured using dopants.

Many fields, including the aerospace industry, have shown increased interest in the use of plastics to lower the mass of systems [3, p. 336]. However, the reasons listed above make the use of plastics challenging for space missions. Therefore, a wide array of testing is typically required to certify novel types of plastic components and structures used in spacecraft. If these challenges can be overcome, secondary spacecraft structures three-dimensionally (3D) printed from doped plastics could offer mass savings in the range of 25–50% for some spacecraft components.

Regarding the specific additive manufacturing (AM) method that has viability for the manufacture of plastics designed for harsh space environments, material extrusion is the method used in this work. Specifically, we focus on fused filament fabrication (FFF) since it is a widespread and low-cost process [4,5]. We foresee extensive use of FFF in future for both terrestrial and in-space manufacturing [6]. The apparent benefit of FFF for in-space manufacturing is that it is well suited for use in a microgravity environment, where powder-based and other AM processes require complex devices. The combination of FFF and atomic layer deposition, for instance, was recently studied by the author [7].

Traditionally, complex-shaped brackets and fittings for spacecraft have been machined from a solid block of high-strength metal. Scrap rates can be up to 80–90% [8]. As part of this work, a clean-sheet design based on AM techniques was utilized to manufacture thermoplastic composite 90° corner brackets with minimal scrap rates. Such brackets can be used to attach subsystems to honeycomb panels in spacecraft. In this work, we report on ground-based testing of corner brackets and some other common GEO satellite parts that we consider could be FFF printed from thermoplastic composites, potentially replacing their metallic baselines.

The paper is organized as follow. First, the 'Materials and methods' chapter describes details on the selected part types and manufacturing. Second, the 'Testing' section explains the methods used for the tests conducted during the work. Finally, we present the results and conclusions.

2. Materials and methods

2.1 The space environment and spacecraft interaction

Space is a challenging environment for man-made devices [9,10,11] posing many difficulties also to polymers. The thermal environment in space changes cyclically due to external conditions, such as an eclipse caused by a planetary body or the attitude taken by the spacecraft. Depending on its mission and location, the operating temperature of different parts of a spacecraft can vary drastically. Some instruments might require cold temperatures close to the cosmic background

  doi:10.5075/epfl-298799_978-2-9701614-0-0

radiation. For example, spacecraft closer to the Sun experience a high thermal influx and might heat up considerably. The heat dumping from a hot polymer part can be helped if the part can conduct heat into thermal sinks. The sunlight, particularly vacuum UV, has a significant impact on a polymer part's structural and surface conditions. Light radiation from the Sun or a planetary albedo is the primary way a spacecraft receives heat. Its internal power usage is another primary source of heating.

The electromagnetic environment poses a challenge by electrostatically charging surfaces exposed to the Sun (see, e.g. [12], and references therein). In the case of polymer parts, this charging can potentially lead to electric discharges, resulting in damage or interference with operation of the spacecraft. The non-light radiation environment (alpha and beta radiation) affects more sensitive components, such as electronics.

The radiation-protection capability of polymers differs from metals, and this needs to be considered when selecting materials. The vacuum environment varies significantly depending on the operational orbit of the spacecraft. However, fairly early in the upper atmosphere, low atmospheric pressure can cause material outgassing. The outgassed material deposits on the spacecraft surface can degrade instrument and sensor performance, with higher material temperatures exacerbating the outgassing of materials.

The printed polymer parts will have to withstand mechanical stresses during the spacecraft mission. Irrespective of the use cases of the polymer parts, arguably the most mechanically stressful part of the mission will be the launch. Specifically, engine-induced vibrations and shocks related to stage separation can damage fragile components. The spacecraft's orbit affects the environment it must withstand. For example, in low-Earth orbits, the thin regions of the atmosphere can degrade polymer parts [13].

2.2 Enhancing the electrical conductivity of filament materials

Whilst enhancing the electrical conductivity of thermoplastics used in FFF, great emphasis must be put on not impairing the compound mechanical properties at the same time. An additional prerequisite on compound design is to allow material printability, preferably with further enhanced printing quality. Mono-functionalized nanodiamond additives allow tailoring of the compound thermal and mechanical properties with minimal material additions. Moreover, such carefully designed compositions allow better printability and, generally, higher quality of the printed item.

2.3 3D printing of test articles

A survey of potential applications was undertaken to understand which polymer parts could potentially replace metal parts inside spacecraft. A trade-off was made by dividing spacecraft parts into different application families and evaluating the amount of potential mass savings, their conductive functions, reduced procurement and logistic efforts, customization, and the specific environmental conditions that the part is expected to endure.

The chosen test articles were: 1) An onboard computer (OBC) electronics enclosure, 2) 90° corner brackets, 3) a radio frequency (RF) circuit housing, and 4) an optical sensor enclosure (Fig. 7).

  doi:10.5075/epfl-298799_978-2-9701614-0-0

The chosen OBC electronics housing was a pre-existing antenna-deployment system housing, which included a hardware mechanical-support frame box with four support frames for circuit boards. The size of the housing was 250 x 148 x 194 mm.

The chosen bracket design was a 90° corner bracket (Fig. 1). It was designed as a generic bracket for providing an attachment point to honeycomb panels. The bracket size was 70 x 35 x 35 mm. The brackets were printed using four different print-layer orientations (*flat, tower*, *porous-face-down,* and *porous-face-up*) as shown in Fig. 2, in order to evaluate the effect of the orientation on the strength of the brackets during testing. Two different mesh types were selected, a diamond and a gyroid mesh. A mesh chosen from these two was used to fill the brackets' interior volume, except for the side faces defined as 4 mm thick solid material. The surface with the largest area was not closed solid. Instead, the mesh was left exposed here. M4 screw holes and openings to insert the screws complement the bracket design. The design accommodates button head screws, for example, Wurth® M4 type 0060 004 16.

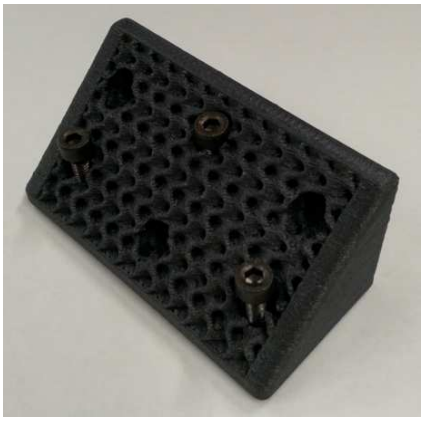

Figure 1. An FFF-printed thermoplastic composite corner bracket. The screw-type was later upgraded to a button-head screw, resulting in better stress distribution within the polymeric material. The bracket features six mounting holes, three for each of the two mounting faces. The additive manufacturing method enables small-batch production of high-stiffness custom-sized and custom-shaped thermoplastic composite brackets.

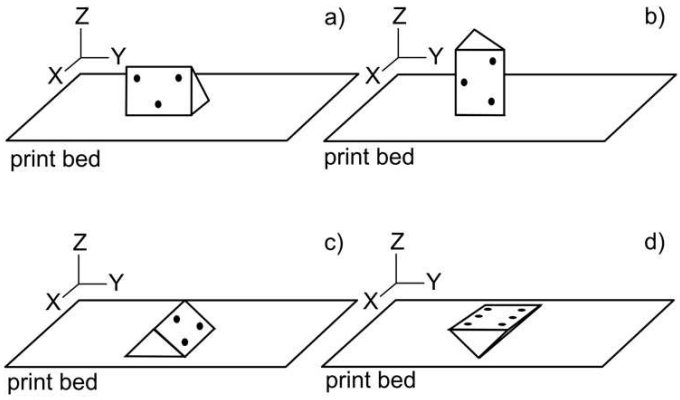

Figure 2. Four possible print-layer orientations for printing the 90° corner brackets used in this work: a) flat, b) tower, c) porous-face-down, and d) porous-face-up.

The chosen radio frequency (RF) circuit housing was a pre-existing RF signal-wire housing. The original housing was machined from aluminium and consisted of two parts, a frame and a lid. The size of the housing was 140 x 67 x 8 mm.

The final test article was an optical sensor enclosure consisting of two parts, a frame, and a dome for an optical sensor. The size of this enclosure was 160 x 165 x 105 mm.

3. Testing

A review of the critical test suite used to qualify space-grade components was conducted at the beginning of the research. Due to the requirements set by the space environment and targeted research outcomes, the following tests were shortlisted: 1) Basic material properties (e.g., tensile strength, Poisson's ratio, density, etc.), 2) thermal cycling, 3) thermal vacuum outgassing, 4) effects of vacuum UV light, 5) vibration test, and 6) manufacturing quality assurance. The following sections contain details of these tests.

3.1 Basic material properties

To enable computer-based loads analysis and finite-element models (FEMs), the basic properties of the material in question need to be investigated when dealing with new materials. In our research, adding dopants into polyether ether ketone (PEEK) necessarily creates a new material with unknown properties. Depending on the level of detail required for the computer-based models, some, or all the properties of the material under study need to be determined. These are well understood at present, and only a few test setups that might be of interest are explained next.

The tensile strength and Poisson's ratio of the new material are derived using a temperature-controlled chamber with a provision to run a tensile load test while an FFF-printed test article is inside the chamber (Fig. 3). The use of liquid nitrogen and heaters allow testing in a temperature range wide enough to qualify components for use in spacecraft.

Figure 3. The chamber used for tensile testing in low and high temperatures at 1 atm.

  doi:10.5075/epfl-298799_978-2-9701614-0-0

For the test of electrical surface conductivity, a special test stand was built (Fig. 4). This stand accepts test articles with the geometry defined by the ISO 527 type 1b standard. The stand has four electrical connections and is built from polycarbonate and Teflon, enabling the use of the stand inside the thermal-vacuum chamber and in 1 atm. The electrical connectors are wired into a Keithley 2701 data acquisition unit which measures the surface conductivity of the test article using the 4-wire resistance measurement method. The unit enables logging of the resistance at set time intervals, allowing the study of how the conductivity changes as a function of ambient pressure and temperature.

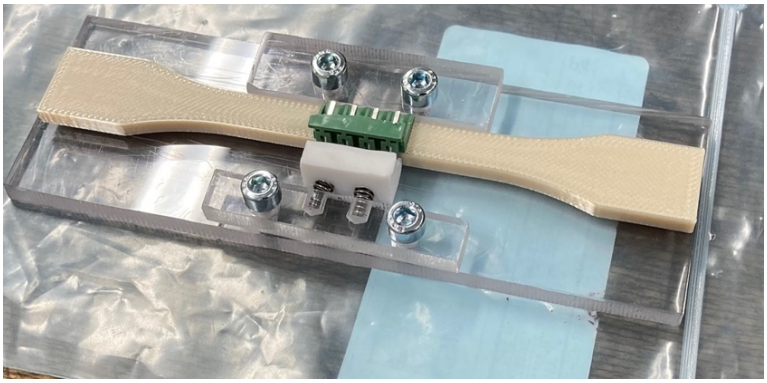

Figure 4. The test stand for performing the 4-wire resistance measurement.

3.2 Thermal cycling

Spacecraft in Earth orbits commonly move in and out of shadow, causing temperature changes due to uneven heating by the Sun. These changes are often cyclical and can be simulated in ground-based testing using environmental chambers (Fig. 5). The thermal cycling test should be conducted in a vacuum for obvious reasons. However, there is always uncertainty regarding the contamination risk of supposedly 'clean' vacuum chambers used for space hardware testing when testing new materials. To manage this risk, the testing was phased so that the new material was first evaluated in the thermal vacuum outgassing test, followed by a thermal cycling test at 1 atm. Based on the analysis of these two tests, the new material under study can be considered safe (or not) for thermal cycling in the vacuum test that follows.

Figure 5. The Espec® chamber for temperature cycling in 1 atm. (left picture), and electrical and data connectors available inside the Aalto Spacelab's thermal vacuum chamber (right picture).

  doi:10.5075/epfl-298799_978-2-9701614-0-0

3.3 Thermal vacuum outgassing

Many materials are unsuitable for use in spacecraft for various reasons, one such reason being the excessive outgassing of volatile material that evacuates the part under vacuum conditions. This outgassing can be further accelerated by heat, commonly generated by the Sun and spacecraft equipment. The reliability of outgassing testing has been questioned in the past. However, processes and instrumentation have improved noticeably in this area. The micro-VCM facility in ESTEC was selected for testing the outgassing behavior of the new material under study.

3.4 Effects of vacuum UV light

Commercial service providers are plentiful for testing materials exposed to UV-A and UV-B light. This is not the case however with regard to the UV-C band due to the requirement of testing in a vacuum [14]. For example, it has been reported that far-ultraviolet (122–200 nm) exposure is a necessary test for assessing the in-space performance of polymer materials [15]. The term "vacuum UV" (VUV) is used extensively in this type of UV testing.

VUV testing of new materials has an inherent risk of contamination. For this reason, a custom-built vacuum chamber (Fig. 6) was selected and modified to incorporate a deuterium lamp. This lamp produces photons in all UV bands and in the visible spectrum, with the peak of the spectrum residing in the UV-C band.

The fact that practically all the UV-C radiation emitted by the Sun is absorbed by the stratospheric ozone allows us to determine the required vacuum level for this test. The atmospheric pressure at 70 km altitude is approximately 5e-2 mb = 5 Pa [16, p. 422], and this was the upper-pressure limit imposed on the vacuum chamber. A typical turbomolecular pump can easily attain this vacuum level. Considering the UV-C attenuation, the amount of air molecules that absorb UV-C still present in the chamber is negligible. The exposure time calculation is based on the acceleration factors (if any) and the requirements set by the space mission in question.

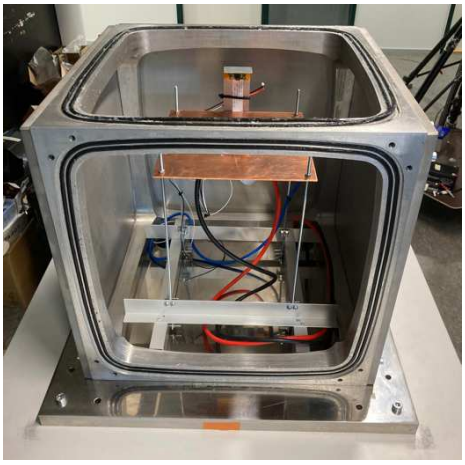

Figure 6. The custom-built "Terrella Cubica" vacuum chamber with one side and the top steel plate removed. The top plate features an opening and a flange for a deuterium lamp. The temperature of samples can be increased by using the resistor-heater attached to the sample holder (copper plate). A camera is installed inside the chamber for monitoring the samples during test runs.

  doi:10.5075/epfl-298799_978-2-9701614-0-0

3.5 Vibration test

The vibration test, also known as the electrodynamic shaker test, seems like a simple verification test. However, this test provides valuable data for the engineers when adequately designed. The natural frequency of parts and assemblies is commonly derived using FEM. The vibration test shows how accurate the FEM is in practice. However, the natural frequencies may differ significantly between the FEM and the actual test. In that case, hardware redesign might be needed to ensure that the natural frequencies of parts and assemblies remain above safe limits during a launch.

Typical vibration tests also include several gentle “sweeps” that produce signature output signals, recorded and later used in the analysis. Any internal damage to the part caused by the high-energy shaking (used to verify the tri-axial launch loads with margins) can be challenging to notice. Conveniently, the signature output measured at the end of the test can be used to detect such failures easily.

Finally, a low-frequency vibration test can be used to create quasi-static loads, enabling a compliance check against static load requirements. The benefit of this approach is that a separate static-load test stand is often not needed. For example, *Ariane 5* load limits are as follows: lateral +/- 2.0 g, axial +4.5 g [17] while in *SpaceX Falcon 9* the values are lateral +/- 2.0 g, axial +6.0 g [18]. The European Cooperation for Space Standardization (ECSS) ECSS-E-ST-32-10C standard defines a factor of 1.25 for the qualification testing of satellite components [19].

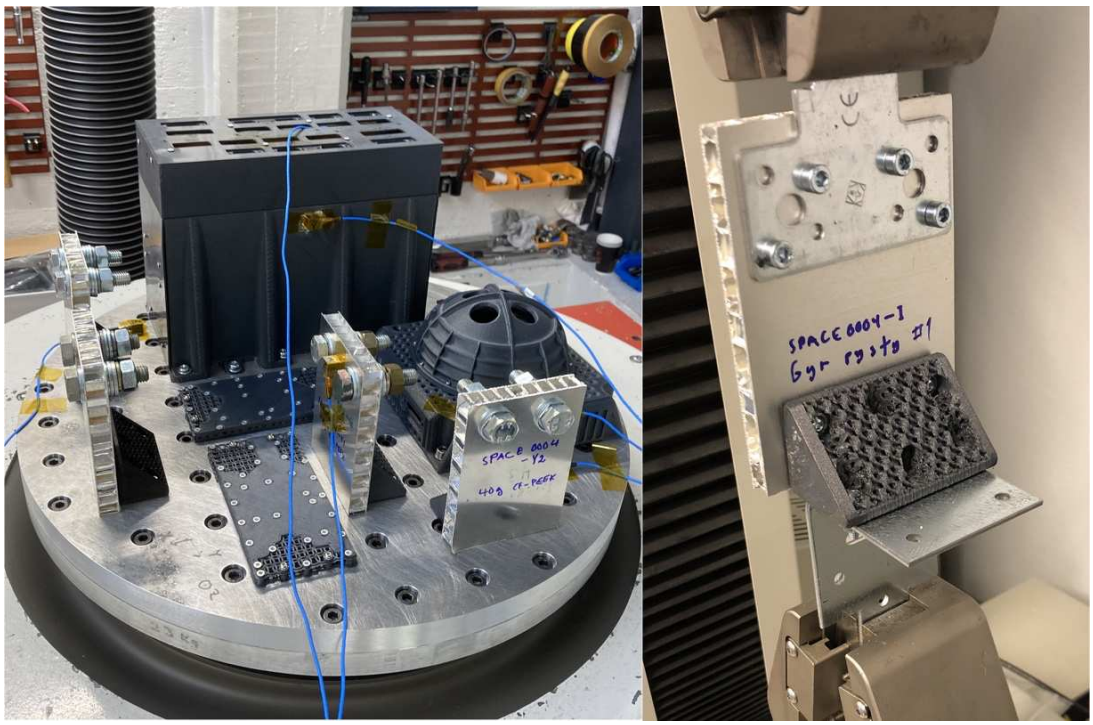

Figure 7. Electrodynamic shaker testing of 3D-printed samples (left). Load testing simulating steady-state acceleration loads was conducted using a tensile load cell. One face of the brackets was attached to a typical aluminium honeycomb panel. The perpendicular face was attached to a steel fixture (right).

  doi:10.5075/epfl-298799_978-2-9701614-0-0

3.6 Corner-brackets load testing

A bracket pull-out test was used to determine the stiffness properties of the corner brackets. The aim was to derive k-values, derived as $k = \Delta F/\Delta l$, where F represents a tensile force (N) and l represents displacement or travel (m). The test was conducted using various bracket designs and materials, including thermoplastics, thermoplastic composites, and aluminium.

3.7 Manufacturing quality assurance

This research determined the quality of FFF-printed parts during and after the manufacturing step. A record of process temperatures, filament-chamber relative humidity and print parameters was stored in a logfile. Deviations from desired values were monitored. Post-manufacturing, the mass and external dimensions of the parts were measured using a microbalance and a vernier caliber. This data was used to plot the x-R charts (Shewhart chart) used in the analysis.

4. Results and discussion

Here, we first describe the design and manufacturing of samples, followed by the test results. The size of the OBC enclosure design created challenges when the design was modified to take advantage of 3D printing while respecting print-chamber size limitations. The OBC enclosure underwent several significant design changes during the iteration process. After trials with the bracket design, two mesh designs (gyroid and diamond) were chosen based on their properties and printability. With these bracket designs, the printing direction affects the strength and durability of the bracket. The brackets printed flat had low strength. The tower and porous-face-down print orientations provided the best results. Strength test results showing brackets made from polylactide (PLA), carbon-fibre doped PEEK and aluminium are shown in Fig. 8. The strength figure-of-merit for the brackets was defined as force divided by bracket mass, where the tensile force (F) is in newtons (N) and applied to the bracket-honeycomb panel joint along one axis as in Fig. 7 (right). The stiffness of the brackets was derived as $k = \Delta F/\Delta l$, where the force (F) is in newtons (N) and the travel (l) is in millimetres (mm). Combining these two parameters to create a plot (Fig. 9) allows the study of the mass-saving enabled by the thermoplastic composite corner brackets.

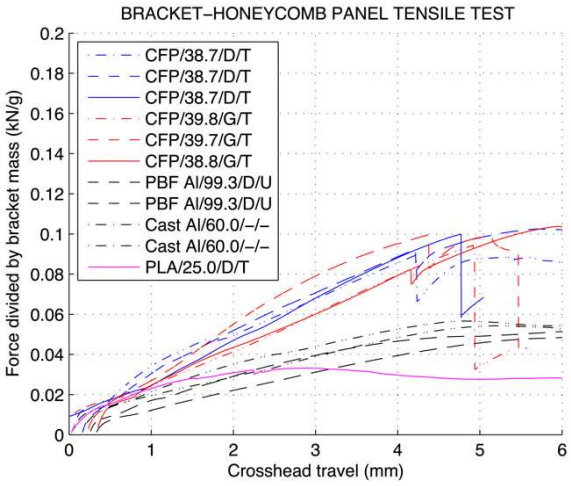

Figure 8. A figure-of-merit (force divided by bracket mass, Y-axis) was used to compare the 90° corner brackets using a tensile load test. The force is in kilonewtons (kN) and the mass in grams

  doi:10.5075/epfl-298799_978-2-9701614-0-0

(g). The X-axis shows the travel of the tensile load cell upper grip, while the lower grip remained stationary. The test article descriptions are as follows. PLA (polylactide thermoplastic using FFF), CFP (carbon-fibre doped PEEK using FFF), PBF AlSi10Mg (aluminium using powder bed fusion), and Cast Al (commercial cast aluminium brackets). Next, bracket mass in grams followed by the mesh type used in the brackets' interior volume ("D" for diamond and "G" for gyroid), and finally the print-layer orientation ("T" for tower, "D" for porous-face-down, and "U" for porous-face-up). The brackets made from carbon-fibre doped PEEK showed good performance.

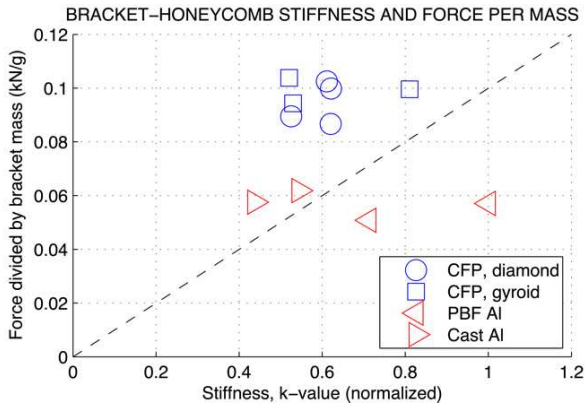

Figure 9. Bracket stiffness (k-value, X-axis) plotted against the force divided by bracket mass figure-of-merit (Y-axis), showing the thermoplastic composite brackets and the powder-bed-fusion (PBF) printed aluminium (AlSi10Mg) baseline bracket. CF-PEEK brackets were FFF-printed using carbon-fibre doped PEEK. The gyroid and diamond refer to the mesh type used in the bracket. A dashed diagonal line shows improved bracket performance when moving right and up.

The RF-housing was redesigned with different meshes to reduce the weight. If the screw positions could be changed from the metallic baseline, further AM-derived mass reduction would be possible. The sensor enclosure was redesigned based on a metallic baseline unit to create new possibilities for similar optical sensor enclosures. The 90-degree corner brackets manufactured using FFF with appropriate settings were demonstrated to have high stiffness and be lightweight, both being highly desirable qualities of a space-grade component. A high k-value corresponds with a structure having a high degree of stiffness.

Doped UV-resistant and AO-resistant plastics are a more robust solution than plastics with a metal oxide coating. That is because coatings are susceptible to pin hole defects, and they lack flexibility.

4.1 Vibration test results

The test articles (Fig. 6) were tested using an electrodynamic shaker in all three axes. The results showed that properly designed structures could fulfill the qualification-level acceleration load requirements commonly applied to spacecraft design. For example, according to these test results, the optical sensor housing would survive a typical launch environment of *SpaceX Falcon 9* and *Ariane 5* rockets.

The natural frequencies of the enclosures were measured and found to be acceptable. The OBC housing enclosure exhibited resonance of the top cover, probably caused by the lack of

  doi:10.5075/epfl-298799_978-2-9701614-0-0

attachment screws in the middle of the cover and the thin shell thickness in that same area. Such shortcomings can be easily overcome by redesigning this part of the enclosure. At the time of writing, a new design has been made and demonstrated with FFF but has yet to be stress-tested.

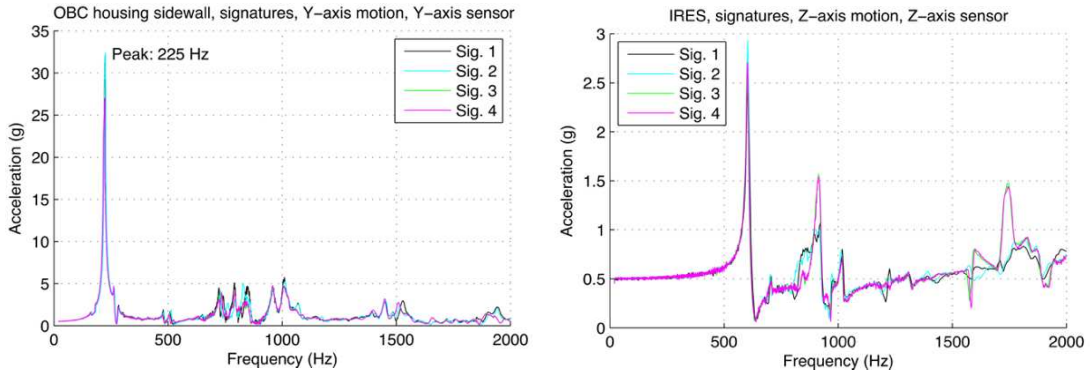

Figure 10. Signature sweep output signals from the OBC housing (left) and optical sensor housing (right), collected during the vibration testing. "Sig. 1–4" refer to four sweeps taken at different phases of testing (before tests, two intermediates, and after tests). These axes had the lowest modal frequencies for these housings. The homogeneity of the signals give proof to the fact that the housing survived the rigors of the test. The highest peak (~225 Hz for the OBC housing and ~600 Hz for the optical sensor housing) shows the natural frequency of the FFF-printed housing. The requirement set for the OBC housing (at least 161 Hz) was fulfilled. Similar requirement for the optical housing was unknown to the authors but was likely met with a good margin. Other axes had higher natural frequencies and are not shown here.

During the research, it became evident that the FEM of the corner bracket and the honeycomb panel joint were more rigid compared to the actual joint based on rivet nuts and screws. This is an excellent example of a case where over-simplification of FEM can lead to problems. On the other hand, detailed FEM of multiple rivet nuts and screws is not feasible due to the severe computing overhead of the simulations (when using desktop computers).

4.2 Results from other tests

Thermal cycling in 1 atm. was completed for three FFF-printed samples, having the shape defined by ISO 527 type 1b and made from nanodiamond doped PEEK (not electrically conducting). The samples were exposed to seven temperature cycles. During these cycles the sample temperatures ranged from -52°C to +144°C. The tensile load test was conducted in room temperature (22°C) in 1 atm. The average tensile strength was 93.98 MPa (SD 0.39 MPa), while the value derived for the tensile modulus was 3.67 GPa (SD 0.05 GPa). Corresponding values for the reference samples (no thermal cycling) were 93.37 MPa (SD 0.12 MPa) and 3.62 GPa (SD 0.02 GPa). At the time of writing, thermal cycling in a vacuum is yet to be done. Regarding the quality assurance, the plotting of Shewhart chart shows promise. However, the data in the charts is highly sensitive to the post processing of FFF-printed parts (cutting and cleaning). The results from the tensile tests in low and high temperatures and from UV-C testing will be published in separate papers. During this work, electrically conducting doped PEEK compound showed a

  doi:10.5075/epfl-298799_978-2-9701614-0-0

degree of conductivity to be classified as 'moderately conductive' according to the ECSS-E-ST-32-10C standard [19]. This material has not yet been FFF-printed.

5. Conclusions

This work showed that the printing parameters used in the FFF process (for example, layer orientation) significantly affect the mechanical performance of the parts. Therefore, that aspect needs to be considered carefully in the design and testing phases.

At present, no clear guidelines exist for the qualification of FFF-printed plastic components for spacecraft [6]. This work fills some of the gaps in this field.

The analysis showed that the FFF-printed carbon-fibre doped PEEK brackets' high strength and stiffness make them ideal for joints used in spacecraft honeycomb panel structures, enabling up to 25–50% savings in bracket mass. The large number of brackets employed in spacecraft structures supports the adoption of this technology. It should also be noted that the material used could also be recycled later when in-orbit FFF-printing becomes standard practice. Furthermore, the used manufacturing method (FFF) enables fast, and cost-effective low batch-size production runs.

Acknowledgements

The authors would like to thank Mr Tomi Kärkkäinen for the design and fabrication of the custom-built "Terrella Cubica" vacuum chamber used in this work.

References

1. Bendsøe MP. Optimal shape design as a material distribution problem. *Structural optimization*. 1989 Dec;1(4):193-202.
2. Zanjanijam AR, Major I, Lyons JG, Lafont U, Devine DM. Fused filament fabrication of peek: A review of process-structure-property relationships. *Polymers*. 2020 Aug;12(8):1665.
3. Kutz M, editor. *Handbook of materials selection*. John Wiley & Sons; 2002.
4. Ait-Mansour I, Kretzschmar N, Chekurov S, Salmi M, Rech J. Design-dependent shrinkage compensation modeling and mechanical property targeting of metal FFF. *Progress in Additive Manufacturing*. 2020 Mar;5(1):51-7.
5. Leach N. 3D printing in space. *Architectural Design*. 2014 Nov;84(6):108-13.
6. Lafont U, Costa M, Rampini, R. Thermoplastics and additive manufacturing: from ground to out-of-earth applications. *In Proceedings of the 2021 European Conference on Spacecraft Structures, Materials and Environmental Testing, ECSSMET 2021, 23–25 March 2021, Virtual.* 2021.
7. Nyman L, Kestilä A, Porri P, Pudas M, Salmi M, Silander R, Miikkulainen V, Kaipio M, Kallio E, Ritala M. Constructing spacecraft components using additive manufacturing and atomic layer deposition: First steps for integrated electric circuitry. *Journal of Aerospace Engineering.* 2021 Sep 1;34(5):04021049. Available from: https://doi.org/10.1061/(ASCE)AS.1943-5525.0001298.
8. Rawal S, Brantley J, Karabudak N. Additive manufacturing of Ti-6Al-4V alloy components for spacecraft applications. *In 2013 6th international conference on recent advances in space technologies*, *RAST 2013, 12–14 Jun 2013, Istanbul, Turkey.* IEEE; 2013. pp. 5-11.

9. Hastings D, Garrett H. *Spacecraft-Environment Interactions*. Cambridge University Press; 2009. Available from: https://doi.org/10.1017/CBO9780511525032.
10. Garrett HB, Whittlesey AC. *Guide to mitigating spacecraft charging effects*. John Wiley & Sons; ISBN: 9781118241332; 2012.
11. Tribble AC. *The Space Environment: Implications for Spacecraft Design - Revised and Expanded Edition*. Princeton University Press; ISBN: 9780691213071; 2020.
12. Ganushkina NY, Swiger B, Dubyagin S, Matéo-Vélez JC, Liemohn MW, Sicard A, Payan D. Worst-Case Severe Environments for Surface Charging Observed at LANL Satellites as Dependent on Solar Wind and Geomagnetic Conditions. *Space Weather*. 2021 Sep; 19(9):e2021SW002732. Available from: https://doi.org/10.1029/2021SW002732.
13. De Groh KK, Banks BA. The MISSE-9 Polymers and Composites Experiment Being Flown on the MISSE-Flight Facility. *In International Space Station Research and Development Conference, ISSR&D 2017, 17–20 Jul 2017, Washington, DC, U.S.A*. 2017 Jul.
14. Johnson RH, Montierth LD, Dennison JR, Dyer JS, Lindstrom ER. Small-scale simulation chamber for space environment survivability testing. *IEEE Transactions on Plasma Science*. 2013 Sep 25;41(12):3453-8.
15. Dever J, Pietromica A, Stueber T, Sechkar E, Messer R. Simulated space vacuum ultraviolet (VUV) exposure testing for polymer films. *In 39th Aerospace Sciences Meeting and Exhibit, 08–11 Jan 2001, Reno, NV, U.S.A*. 2001 Jan. p. 1054. Available from: https://arc.aiaa.org/doi/book/10.2514/MASM01.
16. Chamberlain JW, Hunten DM. Theory of planetary atmospheres, second edition. *Academic Press*; 1987. ISBN: 978-0121672522.
17. Arianespace. *Ariane 5 user's manual issue 5 revision 3*. Arianespace. 2020. Available from: https://www.arianespace.com/wp-content/uploads/2016/10/Ariane5-users-manual-Jun2020.pdf.
18. SpaceX. *Falcon Users Guide September 2021*. SpaceX. 2021. Available from: https://www.spacex.com/media/falcon-users-guide-2021-09.pdf.
19. ECSS (European Coordination for Space Standardization). *European coordination for space standardization*. 2022. Available from: https://www.ecss.nl.

